Environmental Science Processes & Impacts

Characterization of manganese oxide amendments for in situ remediation of mercury-contaminated sediments

Journal:	*Environmental Science: Processes & Impacts*
Manuscript ID	EM-ART-12-2017-000576.R1
Article Type:	Paper
Date Submitted by the Author:	25-Feb-2018
Complete List of Authors:	Leven, Alexander; University of California Merced, Environmental Systems Program Vlassopoulos, Dimitri; Anchor QEA LLC, ; Anchor QEA LLC Kanematsu, Masakazu; Anchor QEA LLC Goin, Jessica; Anchor QEA LLC O'Day, Peggy; University of California Merced School of Natural Sciences,

Characterization of manganese oxide amendments for *in situ* remediation of mercury-contaminated sediments

Alexander Leven[1], Dimitri Vlassopoulos[2], Masakazu Kanematsu[2], Jessica Goin[2], and Peggy A. O'Day[1,*]

[1] Environmental Systems Program, University of California Merced, CA, USA 95343
[2] Anchor QEA, LLC, Portland, OR, USA
* corresponding author email: poday@ucmerced.edu

Environmental Significance Statement

Methylation of inorganic mercury to bioavailable methylmercury poses a complex and challenging problem for mitigation and remediation. Because contamination in sediments or soils is often spread over wide areas at low concentrations, *in situ* treatment rather than removal and disposal is desirable. Manganese(IV) oxide minerals are good candidates for a solid-phase remedial amendment to suppress methylation of mercury by poising porewater oxidation state at a thermodynamic potential higher than sulfate reduction and associated mercury methylation. Experimental investigation of Mn(IV)-oxide amendments to mercury-contaminated sediments and spectroscopic characterization of reaction products followed changes in mineralogy and oxidation state over time to demonstrate mineral redox buffering by mixed-valent (Mn,Fe)(III,II) oxides. Results provide a mechanistic basis for design and application to mercury-contaminated field sites.

Characterization of manganese oxide amendments for *in situ* remediation of mercury-contaminated sediments

Alexander Leven[1], Dimitri Vlassopoulos[2], Masakazu Kanematsu[2], Jessica Goin[2], and Peggy A. O'Day[1,*]

[1] Environmental Systems Program, University of California Merced, CA, USA 95343
[2] Anchor QEA, LLC, Portland, OR, USA
* corresponding author email: poday@ucmerced.edu

Abstract

Addition of Mn(IV)-oxide phases pyrolusite or birnessite was investigated as remedial amendment for Hg-contaminated sediments. Because inorganic Hg methylation is a byproduct of bacterial sulfate reduction, reaction of Mn(IV) oxide with pore water should poise sediment oxidation potential at a level higher than favorable for Hg methylation. Changes in Mn(IV)-oxide mineralogy and oxidation state over time were investigated in sediment tank mesocosm experiments in which Mn(IV)-oxide amendment was either mixed into Hg-contaminated sediment or applied as a thin-layer sand cap on top of sediment. Mesocosms were sampled between 4 and 15 months of operation and solid phases were characterized by X-ray absorption spectroscopy (XAS). For pyrolusite-amended sediments, Mn(IV) oxide was altered to a mixture of Mn(III)-oxyhydroxide and Mn,Fe(III,II)-oxide phases, with a progressive increase in the Mn(II)-carbonate fraction over time as mesocosm sediments became more reduced. For birnessite-amended sediments, both Mn(III) oxyhydroxide and Mn(II) carbonate were identified at 4 months, indicating a faster rate of Mn reduction compared to pyrolusite. After 15 months of reaction, birnessite was converted completely to Mn(II) carbonate, whereas residual Mn,Fe(III,II)-oxide phases were still present in addition to Mn(II) carbonate in the pyrolusite mesocosm. In the thin-layer sand cap mesocosms, no changes in either pyrolusite or birnessite XAS spectra were observed after 10 months of reaction. Equilibrium phase relationships support the interpretation of mineral redox buffering by mixed-valent (Mn,Fe)(III,II)-oxide phases. Results suggest that amendment longevity for redox buffering can be controlled by adjusting the mass and type of Mn(IV) oxide applied, mineral crystallinity, surface area, and particle size. For a given site, amendment capping versus mixing with sediment should be evaluated to determine the optimum treatment approach, which may vary depending on application constraints, rate of Mn(IV) oxide transformation, and frequency of reapplication to maintain desired oxidation state and pH.

Introduction

Mercury and methylmercury pose a significant threat to human and environmental health because of methylmercury bioaccumulation in the food chain. It is estimated that several hundred thousand tons of mercury have been released into the environment during the 20th century alone [1] and atmospheric emissions in the early 21st century are estimated to be around 2000 tons per year [2]. Human and wildlife exposure to mercury is primarily through fish consumption and mostly in the form of methylmercury [2, 3]. The primary pathway for methylation of inorganic mercury is by bacteria as a side reaction during sulfate reduction in anaerobic conditions [4-7], although other bacteria involved in iron reduction and methanogenesis may also methylate mercury [8-10]. In mercury-contaminated environments, however, concentrations of methylmercury are often not correlated with total inorganic mercury concentrations [5, 11], which suggests that either mercury is not available to methylating bacteria, rates of demethylation are high, or environmental conditions do not promote bacterial processes resulting in mercury methylation. Overall, the reduction-oxidation (redox) potential of the sediment-water system controls microbial processes associated with mercury methylation and environmental factors that influence mercury concentrations in sediments.

Methylation of inorganic mercury is prevalent in a variety of environmental settings and poses a widespread, complex, and challenging problem for mitigation and remediation. Very low concentrations of total mercury and methylmercury in sediments (ng/g to μg/g) and water are considered hazardous, and replicate measurements at a given site are often variable and seasonally transient. Contamination is often spread over wide areas such that *in situ* treatments rather than removal and disposal are desirable [12-14]. One strategy for reducing methylmercury concentrations is to manipulate the redox state and/or pH of a system to create conditions unfavorable for sulfate or iron reduction, thus limiting Hg methylation rate. This approach has been employed as part of the remediation plan for mercury at Onondaga Lake, New York through the addition of nitrate to the lake's hypolimnion [15, 16]. A similar approach using liquid calcium nitrate addition to suppress mercury methylation was tested in a pilot project in a dimictic, mesotrophic lake in Minnesota [17]. Monitoring of lake bottom waters showed that nitrate addition raised oxidation potential, suppressed sulfate reduction, and lowered methylmercury concentrations. Once nitrate was depleted, bottom water redox potential decreased as sulfate reduction increased, and methymercury concentrations rose over several weeks [17]. Addition of nitrate, either by intentional dosing or from discharge of treated wastewater, or addition of dissolved oxygen to anaerobic lake bottom waters, has been shown to mitigate methylmercury accumulation [18-21]. These prior studies employed addition to the water overlying anaerobic sediments to suppress mercury methylation, which required repeated dosing or constant discharge to maintain redox conditions at a state higher than favorable for sulfate reduction. An alternative method is the application of a solid phase amendment to mercury-contaminated soil or sediment that similarly poises the local oxidation state at a relatively high level through reaction of the mineral with pore water.

Manganese(IV) oxide minerals are good candidates for a solid-phase remedial amendment to suppress methylation of inorganic mercury. Reduction of Mn(IV) and Mn(III) oxides to Mn(II) occurs at a much higher equilibrium redox potential than that of sulfate reduction [22] and thus creates a thermodynamic "buffer" that energetically disfavors electron transfer among species

with lower equilibrium potentials. These minerals have a variety of polymorphs and related hydrated phases [23], which allows for solids of different surface area, morphology, and reactivity to be selected for specific purposes. They are relatively inexpensive to synthesize or purchase commercially. In natural environments, Mn-oxide minerals are widespread and form readily as a result of coupled chemical and biologically catalyzed pathways in which both bacteria and fungi are known to participate [24, 25]. Their ability to both surface adsorb and incorporate trace metals into their crystal structures are well studied, such that natural Mn oxides are structurally diverse and typically contain a variety of impurities [23, 25-27]. The most common remediation application of Mn oxides has been for removal of dissolved Mn from coal mine drainage waters using aerobic passive flow beds with Mn oxide-coated limestone [28-30]. Natural attenuation of dissolved Mn and other metals through large-scale precipitation of Mn-oxide minerals was documented in the stream hyporheic zone and aquifer at an acid mine drainage site (Pinal Creek, AZ) [31-33]. Degradation of dissolved organic contaminants through oxidation by Mn-oxide surfaces has been examined experimentally but not employed on a large scale [34-36]. To our knowledge, two prior laboratory studies examined two forms of manganese oxide, birnessite (Mn(IV,III) oxide) and manganite (γ-MnOOH), for inhibition of mercury methylation in microbial incubation experiments [37, 38]. Otherwise, Mn(IV) oxides have not been investigated as an *in situ* redox control for sediment or soil treatment of mercury prior to our companion study (Vlassopoulos et al., this issue [39]) and this work.

In this study, two different Mn(IV)-oxide amendments (pyrolusite and birnessite) were investigated as a potential approach to suppress production of methymercury in sediments through redox control of saturated pore water in large-volume sediment mesocosms experiments. Two application strategies, direct mixing of the amendment into sediment or thin-layer sand and amendment caps, were compared. Detailed analysis of the sediment mesocosm experiments, mercury and methylmercury measurements, analysis of the microorganism community, microelectrode voltammetry profiling of sediment porewater, and associated supporting data are given in our companion paper (Vlassopoulos et al., this issue [39]). Briefly, these experimental results showed that porewater methylmercury concentrations in sediments mixed with either pyrolusite or birnessite were reduced by 65-75% relative to an untreated control, and methylmercury concentrations in overlying water were also lower. Mesocosms with sand and amendment caps showed evidence for inhibition of diffusive flux of total mercury and methylmercury to overlying water but sand layers remained oxic. Redox profiles from microelectrode voltammetry indicated the development of reduced zones below amendment-treated sediment layers, with increases in porewater Mn(II) and Fe(II), but no increase in dissolved Mn and Fe concentrations in overlying waters, indicating chemical and/or physical barriers to dissolved fluxes. In this complementary study, X-ray absorption spectroscopy and supporting characterization methods were used to investigate solid-phase manganese speciation in the mesocosm sediments and to evaluate the fate and transformation of the Mn(IV)-oxide amendments over time.

Materials and Methods

Manganese(IV) Oxide Amendments

Two Mn(IV)-oxide amendments were used in the mesocosm experiments. "Acid" birnessite was synthesized as described in [40]. Two moles of concentrated HCl were added dropwise to a boiling solution of 0.25 M $KMnO_4$ (2.5 L) while stirring continuously on a hot plate. After adding HCl, the slurry was boiled for 10 min and then cooled. The resulting precipitate was centrifuged, washed with deionized (DI) water several times to remove excess ions, and then air dried. The specific surface area measured by BET was 48.5±0.3 m^2/g. Manganese dioxide (40/60 mesh powder) as pyrolusite ($Mn(IV)O_2$) was obtained from Laguna Clay Company. The specific surface area measured by BET was 18.7±0.1 m^2/g. The Mn-oxide amendments were characterized using X-ray absorption spectroscopy (XAS) and powder X-ray diffraction (XRD) before reaction in sediment mesocosms.

Sediment Mesocosms

Complete details of the sediment and amendment mesocosm experiments are provided in Vlassopoulos et al. (this issue [39]). Sediment and water chemistry from a mercury-contaminated site are summarized in supplemental information (Tables S1 and S2, respectively). Briefly, experiments were conducted using six 5-gallon glass aquaria (25 cm long × 25 cm wide × 36 cm tall). Previously homogenized marsh sediment was conditioned by saturating with site water amended with acetate (40 mM), yeast extract (1 g/L), and peptone (1 g/L) to stimulate microbial activity. Approximately 8 kg of wet sediment were placed in each aquarium to achieve a sediment depth of 15 cm. An additional 5 cm of material consisting of either sediment or sand with or without Mn(IV)-oxide amendment was added on top of the previously loaded sediment for a total depth of 20 cm. Quartz sand was used for the thin layer (5 cm) cap in three of the six mesocosms. The Mn(IV)-oxide amendments were mixed with added sediment or sand at a dose of 5.0% dry weight. Site water was then carefully added to the mesocosms on top of the sediment until a final water column depth of 15 cm was reached. The overlying water column in each mesocosm was continuously circulated and aerated to maintain dissolved oxygen concentration at air saturation. The mesocosms were kept in the dark except during sampling. Overlying water was periodically added as needed over the course of the experiments to make up for evaporative losses.

The mesocosms were operated for approximately two months prior to initial water sampling to allow steady-state conditions to be established. Sediments were sampled for solid-phase characterizations after about 4 months of operation and sampling was repeated at 10, 13, and 15 months. A small diameter (1 cm) coring tube was used to vertically bore through and retrieve amended layers and underlying sediment samples from the mesocosms. The upper amended sediment or thin-layer sand layer was sectioned off from the underlying sediment, and the subsamples were sealed and frozen until analyses.

Mn K-edge X-ray Absorption Spectroscopy (XAS)

Sediment mesocosm samples were thawed, homogenized by hand, and loaded into Al sample holders and sealed with sulfur-free tape in a glovebox under a gas mixture of 95% N_2 and 5% H_2

in order to prevent oxidation. Samples were analyzed by Mn K-edge XAS at the Stanford Synchrotron Radiation Lightsource (SSRL) on either beamline 4-3 or 4-1. Experimental conditions for XAS data collection are given in Table 1. Energy was calibrated using a Mn foil standard with the inflection on the first absorption peak set at 6539.0 eV. Energy calibration was corrected among spectra collected at different times and experimental conditions to ensure accurate calibration. Multiple scans were collected and averaged using the SIXPack software package [41], with no changes in spectra observed during data collection. Manganese reference compounds (summarized in Table 2) were diluted with either BN or sucrose and collected in either transmission or fluorescence. For both unknown and reference compound spectra, the fluorescence signal was compared with the simultaneously collected transmission signal to check for fluorescence self-absorption (the better of the two was used for analysis). Spectra were analyzed using the Athena software package [42]. Background was subtracted by a linear fit through the pre-edge region and a spline fit through either the extended XANES or the EXAFS regions ($k = 0$ Å^{-1} was set to 6550 eV) and spectra were normalized to the post-edge step height. Spectra were analyzed by least-squares linear combination (LC) fits of reference compound spectra with component weights constrained between 0 and 1 (negative components were rejected) but not forced to sum to unity. All XANES LC fits were done on unsmoothed spectra. Some EXAFS spectra were smoothed using Athena's three-point smoothing algorithm with four iterations to reduce excess noise and provide a better match with reference spectra. Components with a fraction of less than ~10% in the LC fit were removed if they did not significantly improve fit statistics. Reference compound XANES spectra are shown in supplemental information (SI, Fig. S1) and additional details of the XAS data analysis are provided in SI.

Powder X-ray Diffraction (XRD)

Powder XRD data was collected at the Imaging and Microscopy Facility (IMF) at UC Merced or performed commercially at Attard XRD services. Samples collected at the IMF were ground by hand using an agate mortar and pestle and mounted on zero background sample holders. Data was collected on a PANanalytical X'Pert PRO with X'Celerator Detector using a step size of 0.008 from a 2θ value of 5° to 80.2° at 40 kV and 45 mA with a Ni-filtered Co K-α source (λ= 1.78901 Å). Data was converted to Cu K-α wavelength (λ= 1.54439 Å) for analysis and reference pattern matching using X'Pert PRO software and the ICDD PDF-2 database. Background subtraction was carried out using the automatic calculator within the program.

Scanning Electron Microscopy (SEM)

Samples were mounted on Al stubs with carbon tape and imaged in both backscattered and secondary electron modes using a FEI Quanta 200 SEM with a tungsten filament operating at 25 kV voltage and 100 μA emission current. Qualitative elemental analysis of particles in the SEM was done by energy-dispersive X-ray spectrometry with an EDAX Genesis 2000 system.

Results

Mn(IV) Oxide Amendments and Unamended Sediment

Prior to reaction in the mesocosm experiments, Mn(IV)-oxide amendments and unamended sediment from the field site were analyzed to establish initial mineralogy and Mn speciation.

Characterization by powder XRD showed that major reflections in the pyrolusite and birnessite amendments matched reflections in the mineral standards (Fig. 1). The diffractogram for pyrolusite had low signal/noise and a few peaks that appear to be associated with other $Mn(IV)O_2$ polymorphs such as ramsdellite (Fig. 1a). The diffractogram for birnessite had higher counts and distinct reflections, although some peaks were broad and asymmetric, which can be attributed to stacking disorder (Fig. 1b). The birnessite diffractogram was similar to that of acid birnessite reported in Villalobos et al. [43]. Scanning electron microscopy (SEM) images of the Mn(IV)-oxide material showed blocky and rounded particle morphologies for pyrolusite, and a combination of large, platy particles with small particles on surfaces for birnessite (Fig. 2). The pyrolusite particle morphologies are consistent with the lower surface area (18.7±0.1 m^2/g) and low crystallinity observed for pyrolusite compared to birnessite (48.5±0.3 m^2/g).

Comparison of the X-ray absorption spectra of the Mn(IV)-oxide amendments with reference compounds showed that pyrolusite was similar to the spectrum of a synthetic pyrolusite (ß-$Mn(IV)O_2$; [44]), but also showed evidence for another minor component that was matched by a synthetic δ-$Mn(IV)O_2$ ("vernadite" according to [43]) (Fig. 3a). The pyrolusite amendment spectrum was fit best with linear combination of these two $Mn(IV)O_2$ phases. The EXAFS spectrum of the birnessite amendment synthesized in acid conditions was nearly identical to that of synthetic δ-$Mn(IV)O_2$ (Fig. 3a). As discussed in Villalobos et al. [43], acid birnessite is more similar to δ-$Mn(IV)O_2$, with an average Mn oxidation state close to 4, than to Na-birnessite or natural birnessites with K, Na, and Ca substitution and an average Mn oxidation state less than ~3.6 (from a mixture of Mn(IV) and Mn(III)). In contrast, analysis of bulk unamended sediment by XAS showed that Mn speciation in the sediment is dominantly Mn(II). Linear combination fits of the XANES and EXAFS indicated a mixture of Mn(II) carbonate (fit as rhodochrosite) and adsorbed and dissolved Mn(II) species in similar proportions (Fig. 3b).

Characterization of Mesocosm Solids over Time

Pyrolusite Amendment. Characterization of pyrolusite-amended mesocosm sediments by bulk Mn K-edge XAS showed that the unreacted amendment dominated the spectrum after 4 months of reaction, but the presence of a secondary neophase of reduced oxidation state was also detected in addition to Mn^{2+}(aq), likely from pore water (Fig. 4a). The best LC fit of the XANES spectrum was obtained using three reference spectra: unreacted pyrolusite amendment, Mn^{2+}(aq), and jacobsite ($Mn(II)Fe(III)_2O_4$), although the fit to the sediment spectrum was not matched well in the pre-edge region. This result suggests that the neophase likely contained a mixture of Mn and Fe (incorporated from sediment pore water) in a mixed (Mn,Fe)(III,II) oxide phase that was probably not stoichiometric. Estimation of spectral component fractions from normalized XANES LC fits (Table 3) indicated that the mixed-valent oxide phase comprised about 10% of the total Mn absorbance at 4 months. At this low abundance and with evidence for a non-stoichiometric phase, it is likely to have formed as a surface coating on pyrolusite grains.

After 10 months of reaction, the XANES spectrum of pyrolusite-amended sediment was fit best by a combination of a Mn(III)OOH phase (manganite) and Mn(II) carbonate (rhodochrosite) in similar proportions (47% and 41%, respectively), with a smaller fraction of jacobsite (~13%) (Fig. 4a, b; Table 3). The spectrum could not be fit with unreacted pyrolusite. This result shows that the Mn(IV) oxide had been replaced by reduced Mn(III)-oxide and Mn(II)-carbonate phases, with evidence for some incorporation of Fe into the neophases. Analyses of XANES spectra at

13 and 15 months showed that Mn(III) oxide was replaced by Mn(II) carbonate, which dominated the spectral signal. The XANES spectrum at 13 months contained excess pore water with dissolved Mn^{2+}(aq) that masked any minor phases. The spectrum at 15 months was fit mostly by Mn(II) carbonate, but the presence of a mixed-valent oxide phase (fit with jacobsite) was detected in the XANES at about 20% of total Mn (Fig. 4a, b; Table 3). Analysis of the EXAFS spectrum of the 15-month sample confirmed the dominant presence of Mn(II) carbonate (rhodochrosite), but LC fits using reference compounds showed evidence for a mixed-valent oxide phase (Fig. 4c). Unfortunately, no EXAFS spectrum for jacobsite was collected to compare with the sediment EXAFS at 15 months, but features in the sediment spectrum could be fit well with a linear combination of Mn(III)OOH (groutite) and Mn^{2+}(aq). The EXAFS LC result suggests the presence of Mn(III), which cannot be distinguished from Fe as a backscattering atom in EXAFS because of their similar atomic mass ($\Delta Z = 1$). Therefore, the presence of a mixed-valent (Mn,Fe)(III,II)-oxide phase is not ruled out by the EXAFS analysis.

Birnessite Amendment. After 4 months of reaction, analysis of the Mn X-ray absorption spectrum of the birnessite-amended mesocosm sediments showed no evidence for the presence of the original birnessite (Fig. 5a,b). The best LC fit of the XANES spectrum indicated a combination of Mn(II) carbonate (rhodochrosite), Mn^{2+}(aq) (probably mostly from excess pore water), and a Mn(III)OOH phase (manganite) (Fig. 5a,b; Table 3). This result was confirmed by a LC fit to the EXAFS spectrum of this sample, which was fit in approximately the same relative proportions as the normalized XANES spectrum (Fig. 5c). At 10 and 13 months of reaction, LC fits to the sediment XANES spectra showed that Mn(II) carbonate was the dominant component, but the spectral signal also included an intermediate-valent Mn fraction that could be fit with either manganite (Mn(III)OOH), hausmannite ($Mn(II,III)_2O_4$), or a mixture of both (Fig. 5a, b; Table 3). After 15 months of reaction, LC analysis of the sediment XANES indicated the presence of only Mn(II) carbonate (rhodochrosite) at >90% of the total spectrum and minor Mn^{2+}(aq), with no evidence for any oxidized Mn phases (Fig. 5a, b). This result was confirmed by LC analysis of the EXAFS spectrum for this sample, which was well fit with a combination of rhodochrosite and Mn^{2+}(aq) (Fig. 5c). In addition, powder XRD confirmed the presence of crystalline rhodochrosite in the 15-month sediment sample, which was not detected in the X-ray diffractogram after 4 months of reaction (supplemental information Fig. S2). The X-ray absorption spectra were also examined for evidence of precipitation of MnS solid phases. No S ligands could be fit in the EXAFS spectrum of the 15-month sample using shell-by-shell fitting. In Mn-sulfide compounds, S ligands are found at distinctly longer Mn-S distances than Mn-O distances in Mn oxides, and thus should be apparent in the EXAFS if present at a total abundance greater than ~5% of the Mn signal [45].

Amendments Applied in Thin Layer Sand Cap. Pyrolusite and birnessite amendments mixed with sand and applied to sediment as a thin-cap layer in the mesocosms were analyzed by Mn XAS at 4 and 10 months of reaction. Both XANES and EXAFS spectra showed little change over time (Fig. 6). Slight differences in the spectra were due to data collection on different beamlines (Table 1). Thus, the Mn(IV)-oxide amendments were still largely present in their original form 10 months after placement over sediments as a thin sand cap.

Discussion

Transformation of Mn(IV)-oxide Amendments

Characterization of mesocosm solids over time showed that the Mn(IV)-oxide amendments applied directly to sediment were initially transformed into Mn(III) and/or mixed-valent (Mn,Fe)(III,II) hydrous oxide phases over 4 to 13 months. Unreacted pyrolusite still comprised most of the Mn XAS signal at 4 months, but birnessite had already been replaced by Mn(III,II) oxide and Mn(II) carbonate. After 15 months of reaction, the birnessite amendment had been replaced by reduced Mn(II) products, mostly Mn(II) carbonate and a small fraction of aqueous or adsorbed Mn(II), whereas the pyrolusite amendment still showed evidence for a residual mixed-valent (Mn,Fe)(III,II)-oxide phase in addition to Mn(II) carbonate. Linear combination (LC) fits of XANES and EXAFS spectra of the amended sediments with reference compounds that are mostly pure Mn compounds do not uniquely reproduce the experimental data for the mixed valent (Mn,Fe)(III,II)-oxide phases; i.e., different combinations of reference compounds of similar valence and structure can produce acceptable fits. However, the spectral signatures of Mn(IV) oxides, Mn(II) carbonate, Mn(II) sulfide, and aqueous Mn(II) are distinct from that of Mn phases with intermediate or mixed valence and thus readily identified in spectral mixtures. Furthermore, the best LC fits for the pyrolusite-amended sediments consistently included jacobsite ($Mn(II)Fe(III)_2O_4$) as a component over time, whereas the best fits for birnessite-amended sediments were consistently different Mn(III)OOH phases or mixtures that included hausmannite ($Mn(II,III)_2O_4$) rather than jacobsite.

The more rapid transformation of birnessite can be attributed to its higher bulk surface area, plate-like morphology, and the presence of small, poorly crystalline particles associated with a freshly synthesized precipitate. Furthermore, controlled laboratory studies of dissolved Mn(II) reacted with birnessite or other Mn(IV,III) phyllomanganate phases have shown that adsorbed Mn(II) promotes their transformation into Mn(III)OOH phases (feitknechtite, manganite, groutite) and eventually to more thermodynamically stable phases such as hausmannite and/or manganite depending on pH, pe, and solution composition [46-49]. The lower surface area, blocky morphology, and low crystallinity of the pyrolusite amendment helps to explain its slower rate of transformation to Mn(II) products. Interestingly, the slower rate of reaction of the pyrolusite amendment is also associated with XAS spectral evidence for incorporation of Fe into a neophase (fit as jacobsite) noted above, which was not apparent in the reacted birnessite spectra. The formation of jacobsite was identified by XANES as a product in flow-through experiments of MnO_2(s)-coated quartz sand reacted with an Fe(II) solution under acidic conditions [44]. In this study, slower rates of reductive dissolution of MnO_2(s) were attributed to the formation of jacobsite as an armoring surface coating. Redox profiles through the mesocosm sediments after 4 months of reaction using microelectrode voltammetry (Vlassopoulos et al., this issue [39]) showed low dissolved Fe(II) in pore water in the pyrolusite mesocosm over the 0-5 cm depth interval of amended sediment and a sharp increase below 5 cm depth. At this time step, XAS showed evidence for a large fraction of unreacted pyrolusite amendment and the presence of jacobsite. In contrast, dissolved Fe(II) and Mn(II) in pore water in the birnessite mesocosm were generally lower overall throughout the sediment profile, without a sharp distinction between the birnessite-amended sediment layer and unamended sediments below it. The XAS analysis showed no evidence for the presence of the original birnessite amendment at 4 months, and only

Mn(III) and Mn(II) reaction products. The presence of unreacted pyrolusite and a mixed-valent (Mn,Fe)(III,II)-oxide phase together with a well defined redox gradient in the pyrolusite sediment mesocosm indicate maintenance of the redox buffering capacity of the amended layer. The low abundance of the mixed-valent phase estimated from spectral fits and its persistence over time suggest that it may form as surface coatings on pyrolusite grains and perhaps served to further slow the rate of reductive transformation of the Mn(IV)-oxide amendment.

Addition of Mn(IV)-oxide amendments in a sand cap layer showed remarkably little alteration over 10 months of reaction, particularly compared with the relatively rapid reaction of birnessite amended directly into sediments. Results from microelectrode voltammetry (Vlassopoulos et al., this issue [39]) showed the presence of O_2(aq) only in the top 3 cm of the birnessite and sand cap, and in less than the top 1 cm in the pyrolusite and sand cap. Dissolved Mn(II) was low or not detected, and Fe(II) and H_2S(aq) were not detected, in the top 5 cm composed of amendment and sand. Dissolved Mn(II) concentrations increased below 5 cm in both mesocosms, and dissolved Fe(II) was detected below 5 cm in the pyrolusite and sand mesocosm. These redox profiles are likely due to the combination of O_2(aq) diffusing into the porous sand layer from overlying oxygenated water and dissolved Mn(II) diffusing up from reduced sediments below the sand layer that stabilized the Mn(IV)-oxide phases and limited diffusion of dissolved Mn(II) to overlying water (Vlassopoulos et al., this issue [39]). Therefore, placement of Mn(IV)-oxide amendment in a thin-layer sand cap over reduced, methylmercury-prone sediments to create a mixing zone with mildly oxidizing or sub-oxic surface water may be an effective remediation strategy for some sites that prolongs the mineral amendment lifecycle and maintains a relatively high redox potential.

Thermodynamic Constraints

Analysis of the thermodynamic relationships between dissolved and solid phase Mn in the mesocosm experiments suggests that mineral buffering by transformation of the Mn(IV)-oxide amendments was effective in controlling local pore water oxidation state. Measurements of pH and pe in the initial pore water and after 3 and 9 months of reaction were compared with the calculated equilibrium state of the mesocosm sediment experiments at two different total CO_2 concentrations ($pCO_2 = 10^{-3.5}$ or $10^{-4.5}$ atm) (Fig. 7). Initial pH and pe of the water fell within the stability field of Mn^{2+}(aq). After 3 months, pH measured in the birnessite mesocosm pore waters had increased to ~7 and ORP measurements decreased slightly, falling near the intersection of the stability fields of Mn(III)OOH, Mn(II) carbonate (rhodochrosite), and Mn^{2+}(aq) (Fig. 7), which is in agreement with the Mn speciation determined from XAS analysis of amended sediments at 4 months. In the pyrolusite mesocosm, pH increased to ~8 after 3 months and pe was similar to that of the birnessite mesocosm, falling within the stability field of Mn(III)OOH. After 9 months for both mesocosms, pH increased to > 8 and ORP measurements decreased slightly, both now falling near the stability line between Mn(III)OOH and rhodochrosite at higher pCO_2 (Fig. 7a). At pCO_2 lower by an order of magnitude (which suppresses the size of the Mn(II) carbonate field), hausmannite ($Mn(II,III)_2O_4$) is thermodynamically stable and occupies the region between Mn(III)OOH and rhodochrosite (Fig. 7b). The phase relationships compare well with XAS observations of amended sediments at 10 months that showed the presence of Mn(II) carbonate (rhodochrosite) and mixed-valent (Mn,Fe)(III,II) oxide phases, fit as either hausmannite or jacobsite in the XANES LC fits (the pe-pH stability diagrams did not include Fe to simplify calculations). Hausmannite and jacobsite will have similar stability fields

since they are isostructural end-member spinel phases, and electron hopping between Mn(II,III) and Fe(II,III) complicates the assignment of formal oxidation states in these mixed phases[50]. Local microenvironments at mineral surfaces or in pore spaces influenced by microbial metabolisms may have variable levels of pH and dissolved carbonate that may help stabilize different intermediate Mn and Fe phases during system evolution.

The phase relationships suggest that once solids of Mn mixed-valent oxidation state are reduced to Mn(II) only species, mineral buffering would be exhausted and pe would decrease due to sulfate reduction and production of sulfide, at which point mercury methylation linked to sulfate reduction may increase. However, presence of MnS(s) was not observed spectroscopically in the amended sediments after 15 months of reaction, which suggests that levels of sulfide in the amended layers did not increase rapidly after complete conversion to Mn(II) species in the birnessite mesocosm. Furthermore, precipitation of Mn(II) carbonate (rhodochrosite) as a stable phase under reduced conditions provides a thermodynamic pH buffer for the system and controls the dissolved concentration of Mn(II). Dissolved Mn is not regulated as a primary drinking water contaminant, but a secondary standard has been established for taste and smell. High dissolved Mn concentrations such as those found in discharges from acid and coal mining sites can have adverse effects on aquatic systems and beneficial water use [28, 30, 31]. Therefore, at field sites with high dissolved carbonate concentrations, formation of Mn (and Fe) carbonate phases may provide an additional thermodynamic control on system pH and concentration of dissolved Mn.

Conclusions

Large-volume mesocosm experiments operated for up to 15 months demonstrated the potential for Mn(IV)-oxide amendments as a means for sustained redox control of mercury-contaminated sediments. Detailed analysis of the mesocosm experiments and suppression of mercury methylation in Mn(IV)-amended sediments compared to unamended controls are given in a companion paper (Vlassopoulos et al., this issue [39]). Characterization using Mn K-edge XAS of Mn(IV)-oxide amendments and their reaction products over time showed progressive alteration from the original Mn(IV) oxide through intermediate Mn(III)-oxyhydroxide and Mn,Fe(III,II)-oxide phases, with a progressive increase in the Mn(II)-carbonate fraction over time as mesocosm sediments became more reduced. More rapid transformation of freshly synthesized birnessite was associated with higher bulk surface area, plate-like morphology, and the presence of small, poorly crystalline particles compared with a commercially produced pyrolusite of lower bulk surface area and low crystallinity. Comparison of experimental results with theoretical equilibrium phase relationships supports the interpretation that mineral buffering by mixed-valent (Mn,Fe)(III,II)-oxide phases, that are likely to form as surface coatings and include incorporation of Fe from pore water, was the mechanism for poising the sediment-water system at a local oxidation potential above a level favorable for sulfate reduction. General agreement between spectroscopic identification of Mn phases and species, and equilibrium calculations suggest that over the timescale of these experiments, thermodynamic constraints provide a useful framework for directing and evaluating system buffering and evolution given the multiple kinetic reactions, both biotic and abiotic, that control electron transfer among Mn species.

Results suggest that the longevity of a particular amendment treatment for redox buffering can be controlled to some extent by adjustment of the mass and type of Mn(IV)-oxide applied, mineral crystallinity, surface area, and particle size [51, 52]. Comparison of the two different amendment applications indicates that a thin layer sand cap containing Mn(IV)-oxide amendment acts as a physical and chemical barrier to reaction and diffusion, and will have a longer useful lifetime than directly mixing Mn(IV)-oxide into sediment. An important consideration in remedial applications is the mass of amendment needed to maintain a sufficient redox buffering capacity and surface reactivity given the sediment and porewater conditions. Organic compounds and inorganic species may adsorb and be oxidized by Mn(IV)-oxide surfaces, which results in reduction of Mn. At high dissolved concentrations, Mn(II) sorbs to Mn(IV) oxides and drives comproportionation of Mn(II) + Mn(IV) to Mn(III) oxides, followed by further Mn reduction [48, 49, 53, 54]. In general, laboratory studies suggest that maintaining solid phase oxides with mixtures of Mn(IV,III) and slowing production of Mn(II) may help retain surface reactivity and increase the longevity of more oxidized Mn phases. As shown in this study, incorporation of Fe into mixed oxide neophases may provide a surface armoring that slows dissolution of the Mn(IV) oxide and provides additional redox buffering capacity. Amendment capping versus mixing should be evaluated to determine the optimum treatment approach for a given site, which may vary depending on application constraints, rate of Mn(IV) oxide transformation, and frequency of reapplication to maintain desired oxidation state and pH. Periodic exposure of the amended sediment to air may lead to *in situ* regeneration of Mn(IV) oxides, thereby further extending their useful lifetime.

Acknowledgements

The authors would like to thank Estela Reinoso-Maset and Nancy Birkner for assistance with XAS data collection and analysis, and Mike Dunlap, Imaging and Microscopy Facility at UC Merced, for assistance with XRD and SEM. This work was supported by The Dow Chemical Company and UC Merced. Portions of this research were carried out at the Stanford Synchrotron Radiation Lightsource, SLAC National Accelerator Laboratory, supported by the U.S. Department of Energy, Office of Science, Office of Basic Energy Sciences under Contract No. DE-AC02-76SF00515.

Supplemental information: Compositions of sediment and water used in experiments; reference compound XAS, additional details on XAS analysis, and additional XRD data.

References

1. A. W. Andren and J. O. Nriagu, in *The Global Cycle of Mercury*, ed. J. O. Nriagu, Elsevier Biomedical, Amsterdam, 1979, pp. 1–21.
2. C. T. Driscoll, R. P. Mason, H. M. Chan, D. J. Jacob and N. Pirrone, *Environ. Sci. Technol.*, 2013, **47**, 4967-4983.
3. J. M. Hightower and D. Moore, *Environ. Health Perspect.*, 2003, **111**, 604-608.
4. C. C. Gilmour, E. A. Henry and R. Mitchell, *Environ. Sci. Technol.*, 1992, **26**, 2281-2287.
5. J. M. Benoit, C. C. Gilmour, A. Heyes, R. P. Mason and C. L. Miller, in *Biogeochemistry of Environmentally Important Trace Elements*, eds. Y. Cai and O. C. Braids, 2003, vol. 835, pp. 262-297.
6. J. K. Schaefer, S. S. Rocks, W. Zheng, L. Liang, B. Gu and F. M. M. Morel, *Proc. Natl. Acad. Sci. USA*, 2011, **108**, 8714-8719.
7. H. Hsu-Kim, K. H. Kucharzyk, T. Zhang and M. A. Deshusses, *Environ. Sci. Technol.*, 2013, **47**, 2441-2456.
8. E. J. Kerin, C. C. Gilmour, E. Roden, M. T. Suzuki, J. D. Coates and R. P. Mason, *Appl. Environ. Microbiol.*, 2006, **72**, 7919-7921.
9. C. C. Gilmour, M. Podar, A. L. Bullock, A. M. Graham, S. D. Brown, A. C. Somenahally, A. Johs, R. A. Hurt, K. L. Bailey and D. A. Elias, *Environ. Sci. Technol.*, 2013, **47**, 11810-11820.
10. J. M. Parks, A. Johs, M. Podar, R. Bridou, R. A. Hurt, S. D. Smith, S. J. Tomanicek, Y. Qian, S. D. Brown, C. C. Brandt, A. V. Palumbo, J. C. Smith, J. D. Wall, D. A. Elias and L. Y. Liang, *Science*, 2013, **339**, 1332-1335.
11. T. H. Suchanek, C. A. Eagles-Smith and E. J. Harner, *Ecological Applications*, 2008, **18**, A107-A127.
12. C. N. Mulligan, R. N. Yong and B. F. Gibbs, *Journal*, 2001, 193-207
13. P. A. O'Day and D. Vlassopoulos, *Elements*, 2010, **6**, 375-381.
14. F. He, J. Gao, E. Pierce, P. Strong, H. Wang and L. Liang, *Environmental Science and Pollution Research*, 2015, **22**, 8124-8147.
15. D. A. Matthews, D. B. Babcock, J. G. Nolan, A. R. Prestigiacomo, S. W. Effler, C. T. Driscoll, S. G. Todorova and K. M. Kuhr, *Environ. Res.*, 2013, **125**, 52-60.
16. S. G. Todorova, C. T. Driscoll, D. A. Matthews, S. W. Effler, M. E. Hines and E. A. Henry, *Environ. Sci. Technol.*, 2009, **43**, 6572-6578.
17. D. Austin, R. Scharf, J. Carroll and M. Enochs, *Lake and Reservoir Management*, 2016, **32**, 61-73.
18. M. W. Beutel, R. Duvil, F. J. Cubas and T. J. Grizzard, *Water Res.*, 2017, **110**, 288-296.
19. M. Beutel, S. Dent, B. Reed, P. Marshall, S. Gebremariam, B. Moore, B. Cross, P. Gantzer and E. Shallenberger, *Sci. Total Environ.*, 2014, **496**, 688-700.
20. S. R. Dent, M. W. Beutel, P. Gantzer and B. C. Moore, *Lake and Reservoir Management*, 2014, **30**, 119-130.
21. S. A. McCord, M. W. Beutel, S. R. Dent and S. G. Schladow, *Water Resour. Res.*, 2016, **52**, 7726-7743.
22. W. Stumm and J. J. Morgan, *Aquatic Chemistry – Chemical Equilibria and Rates in Natural Waters, 3rd Ed.*, John Wiley & Sons, New York, NY, 1996.
23. J. E. Post, *Proc. Natl. Acad. Sci. USA*, 1999, **96**, 3447-3454.
24. T. G. Spiro, J. R. Bargar, G. Sposito and B. M. Tebo, *Acc. Chem. Res.*, 2010, **43**, 2-9.

25. B. M. Tebo, J. R. Bargar, B. G. Clement, G. J. Dick, K. J. Murray, D. Parker, R. Verity and S. M. Webb, *Annual Review of Earth and Planetary Sciences*, 2004, **32**, 287-328.
26. L. A. J. Garvie, D. M. Burt and P. R. Buseck, *Geology*, 2008, **36**, 215-218.
27. M. A. Marcus, A. Manceau and M. Kersten, *Geochim. Cosmochim. Acta*, 2004, **68**, 3125-3136.
28. C. A. Cravotta and M. K. Trahan, *Appl. Geochem.*, 1999, **14**, 581-606.
29. K. B. Hallberg and D. B. Johnson, *Sci. Total Environ.*, 2005, **338**, 115-124.
30. F. B. Luan, C. M. Santelli, C. M. Hansel and W. D. Burgos, *Appl. Geochem.*, 2012, **27**, 1567-1578.
31. C. C. Fuller and J. W. Harvey, *Environ. Sci. Technol.*, 2000, **34**, 1150-1155.
32. J. T. Kay, M. H. Conklin, C. C. Fuller and P. A. O'Day, *Environ. Sci. Technol.*, 2001, **35**, 4719-4725.
33. C. C. Fuller and J. R. Bargar, *Environ. Sci. Technol.*, 2014, **48**, 2165-2172.
34. J. de Rudder, T. Van de Wiele, W. Dhooge, F. Comhaire and W. Verstraete, *Water Res.*, 2004, **38**, 184-192.
35. J. E. Grebel, J. A. Charbonnet and D. L. Sedlak, *Water Res.*, 2016, **88**, 481-491.
36. C. K. Remucal and M. Ginder-Vogel, *Environmental Science: Processes & Impacts*, 2014, **16**, 1247-1266.
37. T. A. Jackson, *Applied Organometallic Chemistry*, 1989, **30**, 1–30.
38. R. E. Farrell, P. M. Huang and J. J. Germida, *Applied Organometallic Chemistry*, 1998, **12**, 613-620.
39. D. Vlassopoulos, M. Kanematsu, E. Henry, J. Goin, A. Leven, D. Glaser, S. Brown and P. A. O'Day, *Environmental Science: Processes & Impacts*, DOI: 10.1039/C7EM00583K.
40. R. M. McKenzie, *Mineral. Mag.*, 1971, **38**, 493-502.
41. S. M. Webb, *Phys. Scr.*, 2005, **T115**, 1011-1014.
42. B. Ravel and M. Newville, *J. Synch. Rad.*, 2005, 537-541.
43. M. Villalobos, B. Toner, J. Bargar and G. Sposito, *Geochim. Cosmochim. Acta*, 2003, **67**, 2649-2662.
44. J. E. Villinski, P. A. O'Day, T. L. Corley and M. H. Conklin, *Environ. Sci. Technol.*, 2001, **35**, 1157-1163.
45. P. A. O'Day, S. A. Carroll, S. Randall, R. E. Martinelli, S. L. Anderson, J. Jelinski and J. P. Knezovich, *Environ. Sci. Technol.*, 2000, **34**, 3665-3673.
46. K. W. Mandernack, J. Post and B. M. Tebo, *Geochim. Cosmochim. Acta*, 1995, **59**, 4393-4408.
47. J. R. Bargar, B. M. Tebo, U. Bergmann, S. M. Webb, P. Glatzel, V. Q. Chiu and M. Villalobos, *Am. Mineral.*, 2005, **90**, 143-154.
48. E. J. Elzinga, *Environ. Sci. Technol.*, 2011, **45**, 6366-6372.
49. J. P. Lefkowitz, A. A. Rouff and E. J. Elzinga, *Environ. Sci. Technol.*, 2013, **47**, 10364-10371.
50. C. Biagioni and M. Pasero, *Am. Mineral.*, 2014, **99**, 1254-1264.
51. N. Birkner, S. Nayeri, B. Pashaei, M. M. Najafpour, W. H. Casey and A. Navrotsky, *Proc. Natl. Acad. Sci. USA*, 2013, **110**, 8801-8806.
52. H. Peng, I. McKendry, R. Ding, A. Thenuwara, Q. Kang, S. Shumlas, D. Strongin, M. Zdilla and J. Perdew, *Proc. Natl. Acad. Sci. USA*, 2017, **114**, 9523-9528.
53. M. A. G. Hinkle, K. G. Dye and J. G. Catalano, *Environ. Sci. Technol.*, 2017, **51**, 3187-3196.

54. M. A. G. Hinkle, E. D. Flynn and J. G. Catalano, *Geochim. Cosmochim. Acta*, 2016, **192**, 220-234.
55. D. Kinniburgh and D. Cooper, *Phreeplot: Creating graphical output with PHREEQC*, 2011.
56. L. A. J. Garvie and A. J. Craven, *Physics and Chemistry of Minerals*, 1994, **21**, 191-206.

Figure Captions

Figure 1. Powder X-ray diffractograms of Mn(IV)-oxide amendments compared with standard reflections (ICDD PDF-2 database): (a) pyrolusite; (b) birnessite.

Figure 2. Scanning electron micrographs of Mn(IV)-oxide amendments: (a) pyrolusite; (b) birnessite.

Figure 3. Mn K-edge XANES, EXAFS, and Fourier transforms of solids before mesocosm experiments compared with reference spectra. (a) Pyrolusite and birnessite amendments compared with reference compounds pyrolusite (ß -$Mn(IV)O_2$) and vernadite (δ-$Mn(IV)O_2$). Pyrolusite amendment fit (red line) is a liner combination of pyrolusite (ß-$Mn(IV)O_2$) and vernadite (δ-$Mn(IV)O_2$) in nearly equal proportions (spectra scaled in height to their proportions in the fit). The birnessite amendment matches exactly with the vernadite (δ-$Mn(IV)O_2$) reference compound spectrum. (b) Natural sediment from the field site fit (red line) as a linear combination of Mn^{2+}(aq) (smoothed spectrum, ~55%) and rhodochrosite ($Mn(II)CO_3$) (~45%).

Figure 4. (a) Linear combination fits of XANES spectra for mesocosm sediments amended with pyrolusite and reacted for ~ 4, 10, 13, and 15 months. Vertical gray lines indicate the fit range. Data are normalized to the post-edge background. (b) Component percentages from XANES LC fits of reference compounds shown in (a); numerical fit results given in Table 3. (c) Linear combination fit of the EXAFS spectrum and Fourier transform for pyrolusite-amended sediment at 15 months. No EXAFS spectrum was collected for jacobsite ($Mn(II)Fe(III)_2O_4$); the sediment spectrum was fit instead with a combination of Mn(II) (Mn^{2+}(aq), smoothed spectrum) and Mn(III)OOOH (groutite) spectra. Reference compounds are scaled in height to their relative percentages in the fit in both (a) and (c).

Figure 5. (a) Linear combination fits of XANES spectra for mesocosm sediments amended with birnessite and reacted for ~ 4, 10, 13, and 15 months. Vertical gray lines indicate the fit range. Data are normalized to the post-edge background. (b) Component percentages from XANES LC fits of reference compounds shown in (a); numerical fit results given in Table 3. (c) Linear combination fits of the EXAFS spectra and Fourier transforms for birnessite-amended sediment at 4 and 15 months. Reference compounds are scaled in height to their relative percentages in the fit in both (a) and (c).

Figure 6. Mn K-edge XANES, EXAFS, and Fourier transforms of Mn(IV)-oxide amendments mixed with sand and applied as a thin cap layer over sediments, and reacted for the times shown, compared with unreacted amendment; EXAFS spectra were smoothed. (a) pyrolusite; (b) birnessite.

Figure 7. Equilibrium phase relationships in the Mn-O-C-S-H system as a function of pH and pe for the Mn(IV)-amended sediment mesocosm experiments (~total Mn of the experimental system) at two different total CO_2 concentrations (a) $pCO_2 = 10^{-3.5}$ atm (approximately atmospheric concentration); (b) $pCO_2 = 10^{-4.5}$ atm (to suppress the size of the Mn(II) carbonate field). Initial pH and pe of sediment pore water shown (white box); measured pH and pe of

sediment-amended pore water at 3 and 9 months of reaction for pyrolusite (red boxes) and birnessite (blue boxes) mesocosms. Diagram calculated with the program Phreeplot [55].

Table 1. Summary of XAS data collection for mescosm samples.

Sample	Mesocosm Sample Date	XAS Collection Date	Temp [1]	Beamline	Focusing Mirror	Mono[2]	Detector[3]	Soller Slits
Bir (unreacted) [4]	--	3/5/2015	RT	4-3	Ni	Si(111)	Transmission	n.a.
Pyr (unreacted) [4]	--	1/7/2016	LN2	4-3	Ni	Si(111)	SDD	Y
Sed (unamended)	--	1/7/2016	LN2	4-3	Ni	Si(111)	SDD	Y
Bir Sed (4 mo)	7/7/2015	7/11/2015	RT	4-3	Ni	Si(111)	PIPS	N
Pyr Sed (4 mo)	7/7/2015	7/11/2015	RT	4-3	Ni	Si(111)	PIPS	N
Bir Sand (4 mo)	7/7/2015	7/11/2015	RT	4-3	Ni	Si(111)	PIPS	N
Pyr Sand (4 mo)	7/7/2015	7/11/2015	RT	4-3	Ni	Si(111)	PIPS	N
Bir Sed (10 mo)	1/4/2016	1/7/2016	LN2	4-3	Ni	Si(111)	SDD	Y
Pyr Sed (10 mo)	1/4/2016	1/7/2016	LN2	4-3	Ni	Si(111)	SDD	Y
Bir Sand (10 mo)	1/4/2016	1/7/2016	LN2	4-3	Ni	Si(111)	SDD	Y
Pyr Sand (10 mo)	1/4/2016	1/7/2016	LN2	4-3	Ni	Si(111)	SDD	Y
Bir Sed (13 mo)	4/16/2016	4/22/2016	LN2	4-1	none	Si(220)	Ge	N
Pyr Sed (13 mo)	4/16/2016	4/22/2016	LN2	4-1	none	Si(220)	Ge	N
Bir Sed (15 mo)	6/24/2016	7/8/2016	LN2	4-1	none	Si(220)	Ge	Y
Pyr Sed (15 mo)	6/24/2016	7/8/2016	LN2	4-1	none	Si(220)	Ge	Y

[1] RT: room temperature; LN2: sample held in liquid N_2 cryostat

[2] Double-crystal monochromator

[3] Cr 3-μT filter used with fluorescence detectors; SDD: Silicon drift detector (4-element Hitachi Vortex ME-4); PIPS: passivated implanted planar silicon; Ge: solid-state multi-element germanium (Canberra)

[4] Diluted with sucrose

Table 2. Manganese reference compounds used for XAS analysis.

Compound	Formula	Source [a]	Data Collection	Reference [b]
Pyrolusite	ß-$Mn^{IV}O_2$	syn	transmission	1
Ramsdellite	γ-$Mn^{IV}O_2$	nat	fluorescence	2
Vernadite	δ-$Mn^{IV}O_2$	syn	transmission	3
Na-Birnessite	$Na_{0.26}(Mn^{IV}_{0.27}Mn^{III}_{0.26})O_2$	syn	transmission	3
Birnessite	$(Na,Ca,K)_x(Mn^{IV}Mn^{III})_2O_4 \cdot yH_2O$	nat	transmission	4
Groutite	α-$Mn^{III}OOH$	nat	fluorescence	5
Manganite	γ-$Mn^{III}OOH$	nat	transmission	6
Bixbyite	$Mn^{III}_2O_3$	nat	fluorescence	7
Jacobsite	$Mn^{II}Fe^{III}_2O_4$	syn	fluorescence	8
Hausmannite	$Mn^{II}Mn^{III}_2O_4$	syn	transmission	9
Rhodochrosite	$Mn^{II}CO_3$	nat	transmission	10
MnS(s)	$Mn^{II}S$	syn	transmission	11
Mn^{2+}(aq)	Mn^{2+}(aq)	syn	fluorescence	12

[a] syn: synthetic; nat: natural

[b] (1) Villinski et al. [44]; (2) Pirika mine, Hokkaido, Japan [56]; (3) Villalobos et al. [43]; (4) Birness, Scotland, collection of L. Garvie; (5) Navajo County, AZ, USA, collection of L. Garvie; (6) Ironton, MT, USA, Ward's Scientific; (7) Thomas Mountain, UT, USA, collection of L. Garvie; (8) Villinski et al. [44]; (9) Bargar et al. [47]; (10) Catamarca Province, Argentina, Ward's Scientific; (11) Amorphous precipitate [45]; (12) 10 mM $MnSO_4$ solution [44].

Table 3. Results of linear combination fits of XANES spectra of amended mesocosm sediments.

Sediment Amendment	Reaction time (months)	Unreacted amend-ment	Manganite (γ-$Mn^{III}OOH$)	Jacobsite[a] ($Mn^{II}Fe^{III}_2O_4$)	Hausmannite[a] ($Mn^{II}Mn^{III}_2O_4$)	Rhodochrosite ($Mn^{II}CO_3$)	Mn^{2+} (aq)[b]	Total	Reduced χ^2 ($*10^{-4}$) [c]	R-factor ($*10^{-4}$)[d]
Pyrolusite	4	72.6		9.7			19.1	101.4	2.4	3.0
	10		47.2	12.9		40.7		100.8	1.4	1.7
	13					52.0	49.5	101.5	6.1	6.7
	15			23.6		77.0		100.6	8.8	10.
Birnessite	4		11.3			38.3	51.5	101.1	4.4	4.9
	10				32.4	70.1		102.5	8.6	3.9
	13		23.3		21.9	54.3		99.5	6.4	8.0
	15					92.8	8.6	101.4	18	20.

[a] Jacobsite and hausmannite are ideal end-member compositions of isostructural spinel phases; Mn(II,III) and Fe(II,III) commonly mix in structural sites.

[b] Samples wet during data collection

[c] Reduced χ^2 : statistical goodness-of-fit equal to (F-factor) / (# of points - # of variables)

[d] R-factor: statistical goodness-of-fit equal to ($\sum$ (data-fit)^2 / $\sum$ (data)^2)

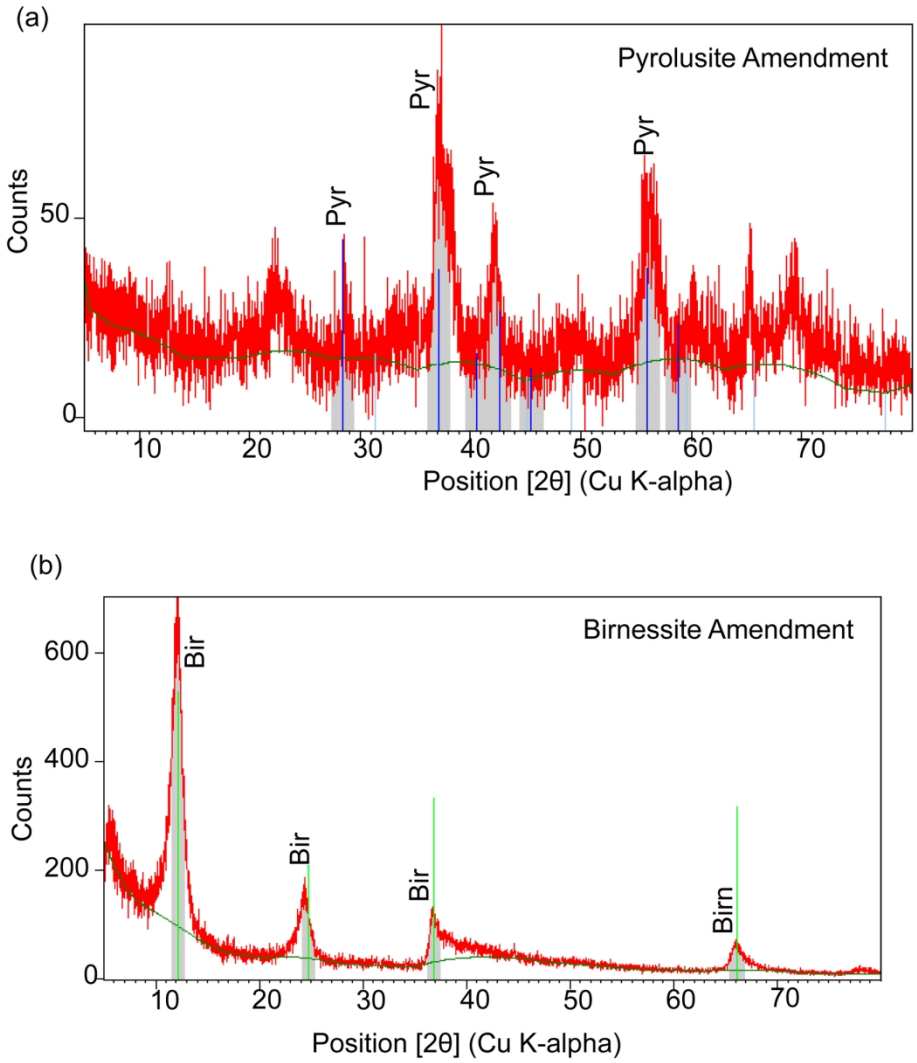

Figure 1

156x193mm (300 x 300 DPI)

(a) Pyrolusite amendment

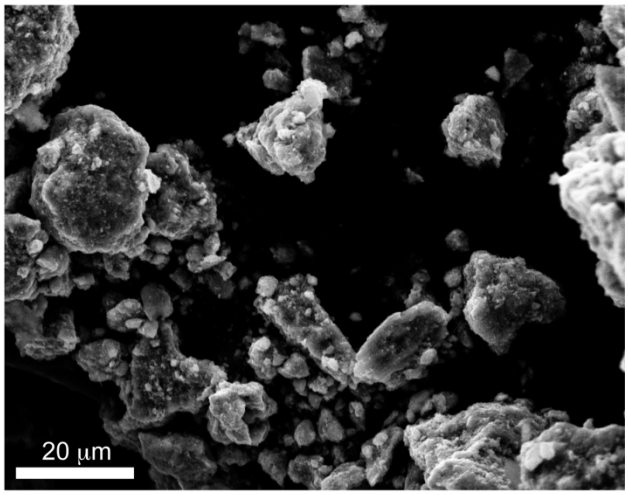

(b) Birnessite amendment

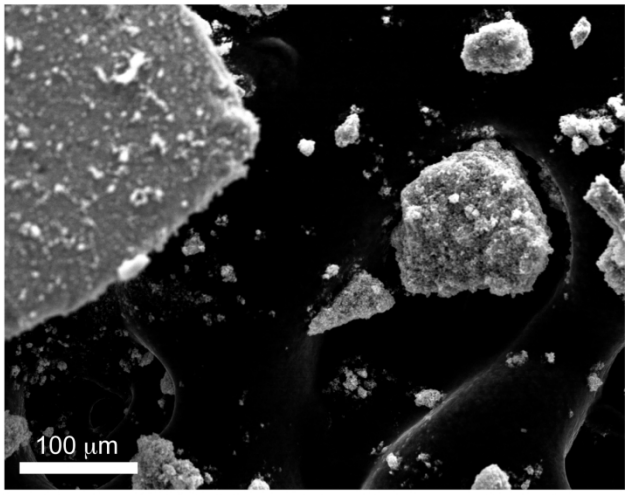

Figure 2

135x261mm (300 x 300 DPI)

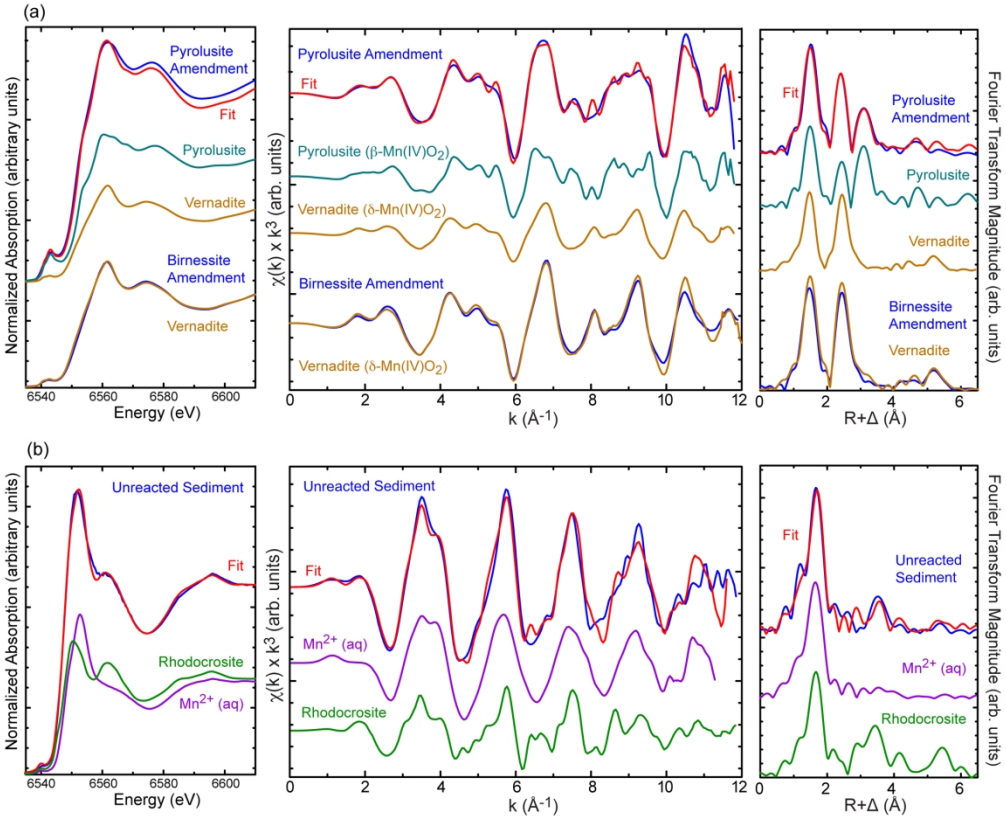

Figure 3

179x165mm (300 x 300 DPI)

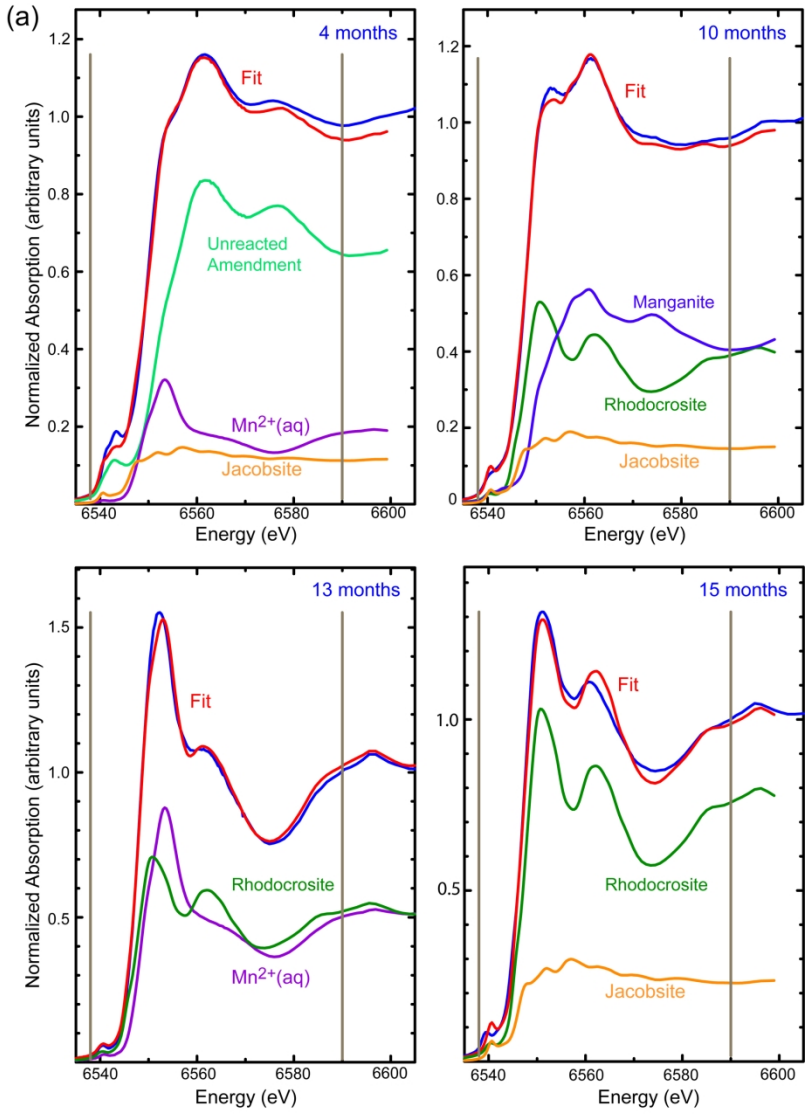

Figure 4

186x253mm (300 x 300 DPI)

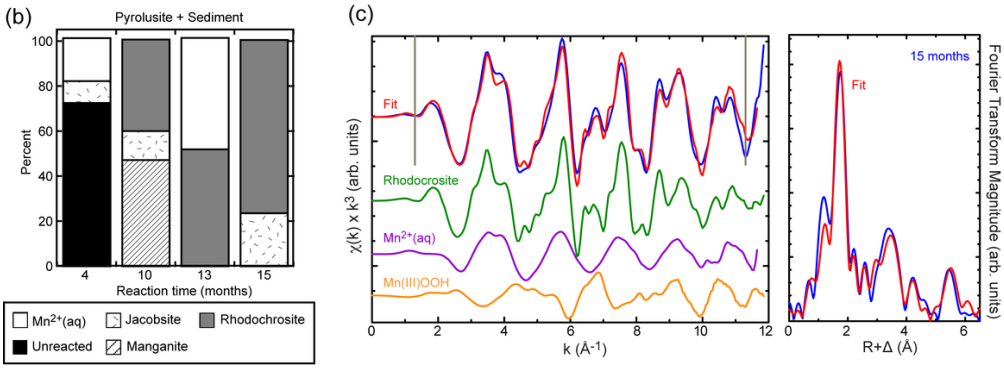

Figure 4

98x49mm (300 x 300 DPI)

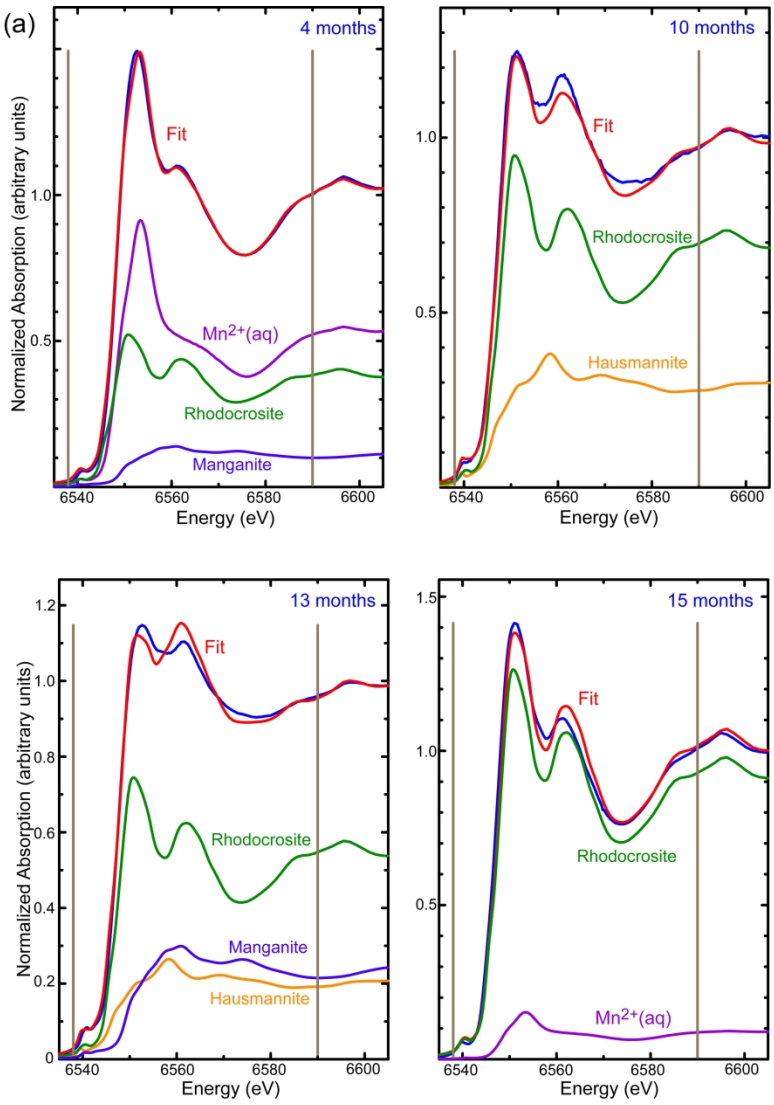

Figure 5

192x299mm (300 x 300 DPI)

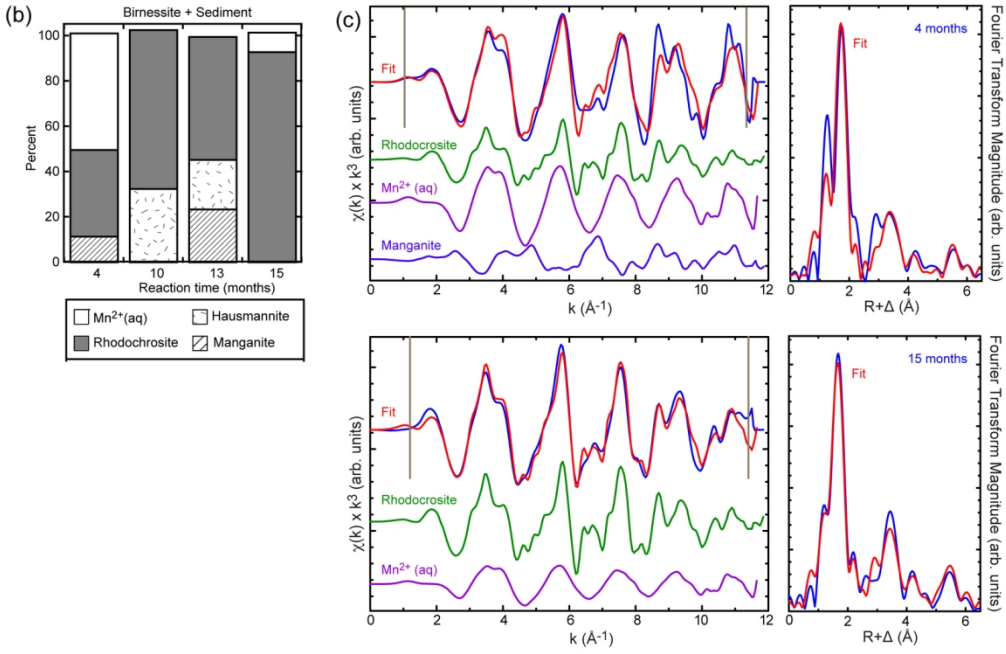

Figure 5

138x99mm (300 x 300 DPI)

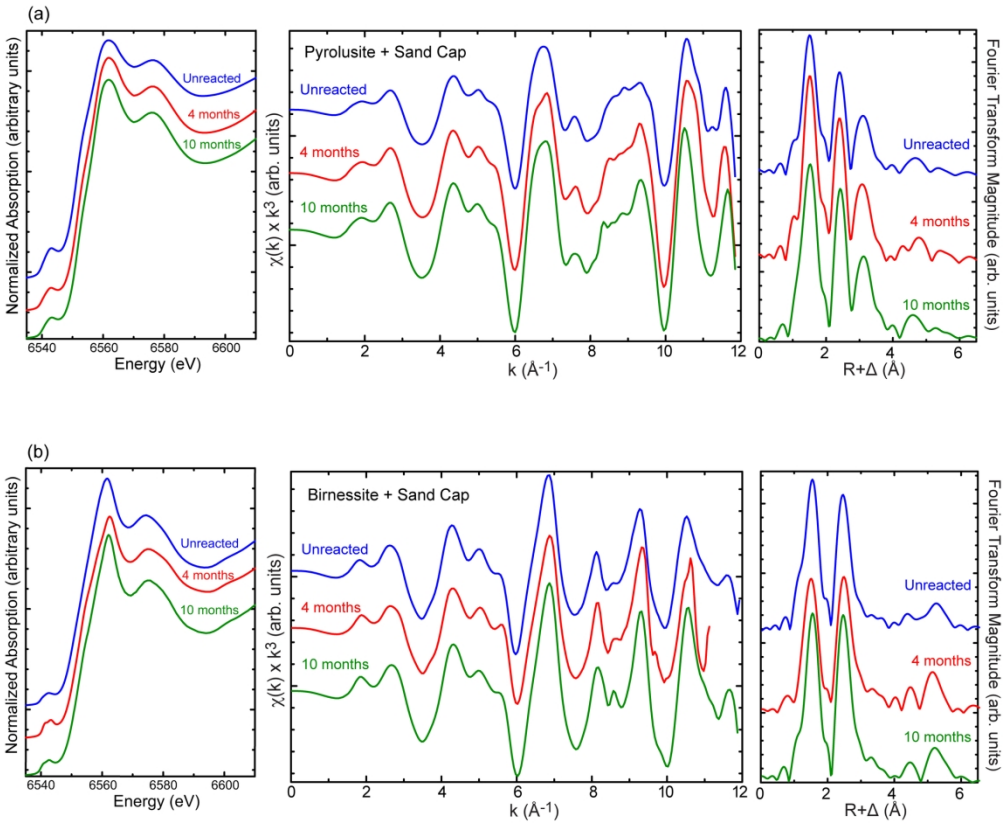

Figure 6

180x166mm (300 x 300 DPI)

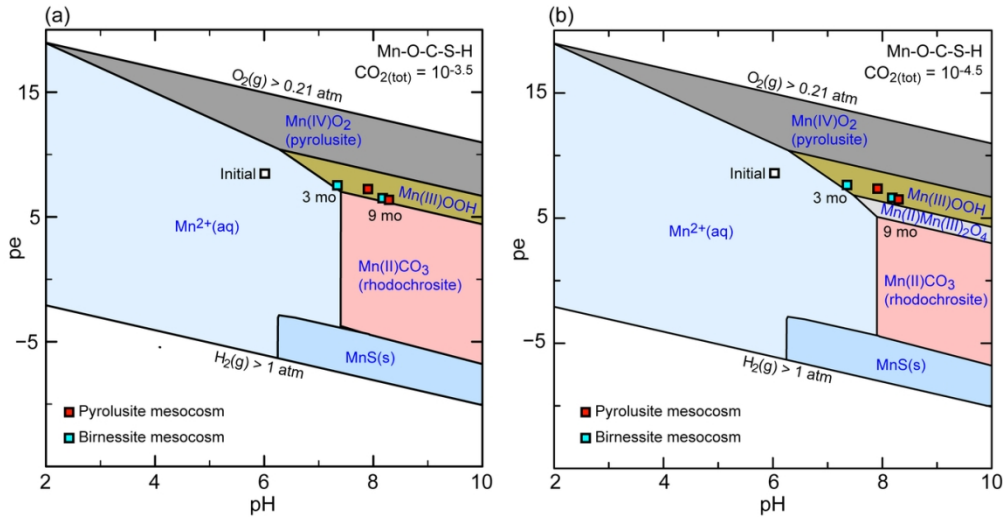

Figure 7

115x65mm (300 x 300 DPI)

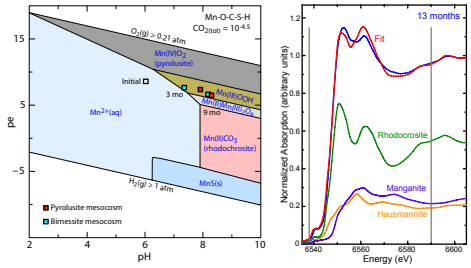

Mn(IV)-oxide amendment experiments with mercury-contaminated sediments demonstrate mineral redox buffering by mixed-valent (Mn,Fe)(III,II) oxides to limit mercury methylation.